

# Reliable data clustering with Bayesian community detection

Magnus Neuman,\* Jelena Smiljanić,† and Martin Rosvall  
*Integrated Science Lab, Department of Physics, Umeå University, Umeå, Sweden*  
(Dated: October 20, 2025)

From neuroscience and genomics to systems biology and ecology, researchers rely on clustering similarity data to uncover modular structure. Yet widely used clustering methods, such as hierarchical clustering,  $k$ -means, and WGCNA, lack principled model selection, leaving them susceptible to noise. A common workaround sparsifies a correlation matrix representation to remove noise before clustering, but this extra step introduces arbitrary thresholds that can distort the structure and lead to unreliable results. To detect reliable clusters, we capitalize on recent advances in network science to unite sparsification and clustering with principled model selection. We test two Bayesian community detection methods, the Degree-Corrected Stochastic Block Model and the Regularized Map Equation, both grounded in the Minimum Description Length principle for model selection. In synthetic data, they outperform traditional approaches, detecting planted clusters under high-noise conditions and with fewer samples. Compared to WGCNA on gene co-expression data, the Regularized Map Equation identifies more robust and functionally coherent gene modules. Our results establish Bayesian community detection as a principled and noise-resistant framework for uncovering modular structure in high-dimensional data across fields.

## I. INTRODUCTION

Researchers apply clustering techniques to analyze similarity data from diverse systems [1] such as the human brain [2, 3], ecological assemblages [4–6], the regulatory mechanisms of genes [7, 8], and plant-pathogen interactions [9]. Despite their diversity, the common goal is to partition observed features based on their similarity to identify meaningful clusters and uncover underlying organization. For instance, species co-occurrence data can reveal species groups sharing similar environmental conditions, and gene expression patterns can reveal clusters of genes with similar functions.

The sheer number of pairwise associations in high-dimensional data threatens to drown signal in noise [10]. When researchers apply clustering methods directly to unfiltered data or similarity matrices, noise, outliers, and arbitrary parameters obscure the clusters [11, 12]. Current approaches tackle this challenge in two disconnected steps: first reducing noise, then finding clusters [13–15]. This separation creates fundamental problems.

One class of methods first compresses high-dimensional data into fewer dimensions, often with PCA [16] or UMAP [17], then applies clustering algorithms such as  $k$ -means [15, 18] or hierarchical clustering [13]. This two-step process creates multiple problems. First, researchers must make arbitrary choices twice: how many dimensions to keep and how many clusters to find. Second, the dimensionality reduction may discard information that defines clusters while preserving variance that reflects noise [11, 19, 20]. Third, these methods can detect clusters even when there is no modular structure in the under-

lying data [12]. The root problem: the reduction step determines what the clustering step can possibly find, yet operates blind to the clustering objective.

Another class of methods first sparsifies correlation matrices through thresholding, then applies clustering algorithms [21–23]. Researchers compute pairwise correlations between all features, typically using Pearson correlation. Accurately estimating these correlations requires many samples relative to the number of features [24]. However, this requirement rarely holds in practice. For example, gene co-expression studies demand expensive and time-consuming gene sequencing experiments [25], while ecologists contend with detection errors and resource constraints when collecting plant occurrence data across field plots [26]. With scarce data yielding unreliable correlations, researchers sparsify these noisy matrices into networks where features form nodes and correlations above a chosen threshold form links [27]. This hard thresholding opens access to powerful network algorithms, including community detection methods for clustering.

Sparsification seeks to reduce noise but optimizes for networks, not clusters. While finding accurate links and finding reliable clusters require different objectives [28–31], most clustering pipelines apply thresholding without theoretical justification, based on various heuristic network criteria [23, 32]. Each threshold creates a different network: lower thresholds retain noise in dense networks; higher thresholds remove signal in sparse networks. Even the all-in-one package WGCNA (Weighted Gene Correlation Network Analysis) with its soft thresholding based on scale-free topology [21, 33] optimizes for network accuracy before clustering. When sparsification predetermines what clustering can detect, unreliable correlations can produce distorted clusters.

For reliable clustering of noisy data, we must unite sparsification and clustering in a single principled step using clusters themselves as the model selection crite-

\* magnus.neuman@umu.se

† Also at Scientific Computing Laboratory, Center for the Study of Complex Systems, Institute of Physics Belgrade, University of Belgrade

riion. Triangles illustrate why network and cluster optimization diverge. While triangular patterns often preserve or even enhance modular structure, graphical lasso [39, 40] and other partial correlation methods [41, 42] specifically identify these patterns as indirect associations and remove them to improve network accuracy. For our clustering objective, such network-focused precision adds no value. For example, we previously demonstrated that cross-validating based on cluster quality instead of network accuracy produces networks that better reveal modular structure, whether applied directly to correlation networks [31] or to graphical lasso [34]. These cluster-focused optimizations succeed because mesoscale clusters remain robust across reasonable threshold ranges when genuine modular structure exists: clusters tolerate both missing and spurious links within bounds [31, 35–38]. While the cross-validation approaches aim to find the sparsest networks that preserve modular structure, they waste already scarce samples on validation instead of using them for inference.

To optimize the modular structure while preserving all samples for inference, we leverage Bayesian community detection methods developed for noisy data [37, 38, 43, 44]. Using the Minimum Description Length (MDL) principle [45] to balance model complexity against fit, these methods resolve the trade-off between collapsed clusters from low-threshold dense networks and fragmented clusters from high-threshold sparse networks. They find the partition that best compresses the observed data, automatically determining the number of clusters. This one-step approach transforms how we detect clusters with three key advantages: First, it replaces two arbitrary choices – threshold value and cluster number – with MDL-based compression as one principled criterion. Second, it preserves all samples for inference instead of wasting data on cross-validation. Third, it refuses to impose structure on pure noise, returning a single cluster when no modular structure exists.

While we focus on the Pearson correlation here, our approach extends to other similarity measures, including mutual information and maximal information coefficient [46], and field-specific measures such as molecular or species similarity [47, 48]. It also applies directly to similarity networks without requiring the underlying samples. We evaluate two Bayesian methods for community detection: the Degree-Corrected Stochastic Block Model (DC-SBM) [43] and the Regularized Map Equation [38] implemented in Infomap [49], chosen for their proven accuracy.

We find that our one-step approach enables more accurate and robust cluster detection in similarity data and correlation networks, especially when data are limited or noisy, the common reality in experimental research. By analyzing correlation distributions in synthetic datasets with known cluster structure, we show how detectability depends on noise level, sample size, correlation strength, and number of clusters. Our one-step approach outperforms traditional methods, with the Regularized Map

Equation recovering planted partitions even under high noise. Compared to the widely used WGCNA on gene co-expression data from the Allen Human Brain Atlas, the Regularized Map Equation identifies more robust and functionally coherent gene modules.

## II. CORRELATION DISTRIBUTIONS

Detecting clusters in similarity data requires distinguishing structured associations from background noise. Distinguishing signal from noise becomes especially challenging when the data are limited, the correlations are weak, or the underlying structure is fine-grained. We analyze how the distributions of within-cluster and outside-cluster correlations relate to one another, and how this relationship depends on sample size, population correlation strength, and the number of clusters.

When the cluster signal is sufficiently strong, within-cluster correlations will, on average, exceed those between features from different clusters. Recovery of the underlying structure depends on how well these two distributions are separate. While this separation naturally depends on the population correlation strength, other model parameters such as the number of samples, features, and clusters also influence the separation.

To assess the detectability of modular structure in correlational data, we first analyze synthetic datasets that allow us to characterize correlation distributions under controlled conditions. We generate synthetic data using a stochastic block model adapted for correlational data, with  $N$  observed features in  $q$  planted clusters of equal size. To control the noise level in the observed correlations, we vary both the strength of the planted population correlation  $\rho$  between features in the same cluster and the number of samples  $L$ . We sample data  $X \in \mathbb{R}^{L \times N}$  from a multivariate normal distribution, such that  $X \sim \mathcal{N}(0, \Sigma)$ , where the covariance matrix  $\Sigma$  has block structure:

$$\Sigma_{ij} = \begin{cases} \rho, & \text{if } i \text{ and } j \text{ belong to the same cluster,} \\ 0, & \text{otherwise.} \end{cases} \quad (1)$$

The observed correlation matrix  $\hat{\Sigma} = X^T X / (L-1)$  serves as our input for cluster inference. With enough samples and strong population correlation, this matrix reveals the planted structure (Fig. 1A). The number and sizes of clusters also influence detectability: small clusters cover a smaller portion of the covariance matrix and yield fewer within-block correlation samples, producing noisier estimates of the within-cluster correlation distribution.

To clarify the inference problem, we consider the distribution  $f(r; \rho, L)$  of correlation  $r$ , which has a known

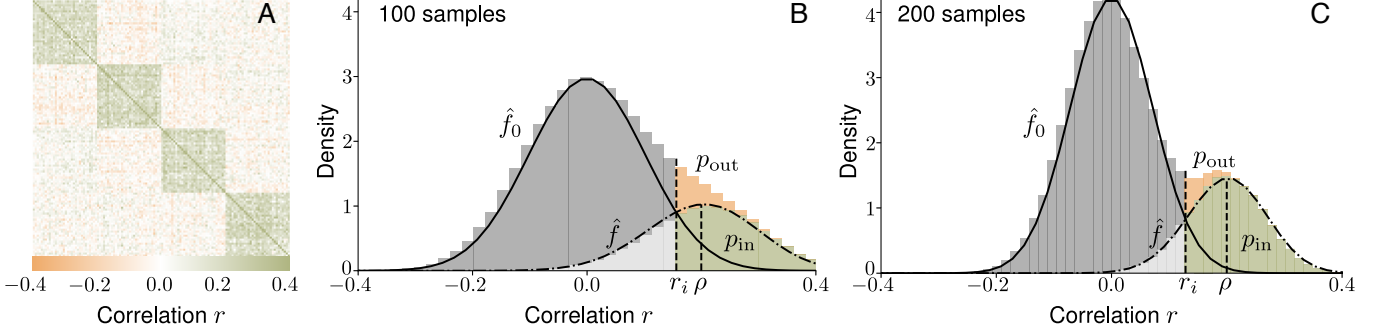


FIG. 1. **Overlapping correlation distributions.** In A, the planted structure is visible in the observed correlation matrix  $\hat{\Sigma}$ , since the within-cluster correlations on average exceed the outside-cluster correlations. This separation depends on the number of samples, nodes, and clusters, and on the population correlation  $\rho$ . Colorbar truncated at 0.4; diagonal entries have correlation 1. With few samples in B, the within- and outside-cluster distributions  $\hat{f}$  and  $\hat{f}_0$  overlap, and the number of false positives using the threshold  $r_i$ , where  $\hat{f}_0$  and  $\hat{f}$  intersect, is relatively large, making correct inference difficult. With more samples in C, the situation becomes more favorable. The fractions of within- and outside-cluster correlations above  $r_i$  are  $p_{in}$  (green, true positives) and  $p_{out}$  (orange, false positives) respectively.

analytical expression derived by Hotelling [50]:

$$f(r; \rho, L) = \frac{(L-2)\Gamma(L-1)(1-\rho^2)^{\frac{L-1}{2}}(1-r^2)^{\frac{L-4}{2}}}{\sqrt{2\pi}\Gamma(L-\frac{1}{2})(1-\rho r)^{\frac{2L-3}{2}}} {}_2F_1\left(\frac{1}{2}, \frac{1}{2}, \frac{2L-1}{2}, \frac{\rho r+1}{2}\right), \quad (2)$$

where  $\Gamma(z)$  is the gamma function and  ${}_2F_1(a, b, c, d)$  is Gauss' hypergeometric function. For uncorrelated data,  $\rho = 0$ , and the distribution reduces to

$$f_0(r; L) = \frac{(L-2)\Gamma(L-1)(1-r^2)^{\frac{L-4}{2}}}{\sqrt{2\pi}\Gamma(L-\frac{1}{2})} {}_2F_1\left(\frac{1}{2}, \frac{1}{2}, \frac{2L-1}{2}, \frac{1}{2}\right). \quad (3)$$

The modular structure scales the correlations into distributions  $\hat{f}(r; \rho, L, q, N)$  and  $\hat{f}_0(r; L, q, N)$ :

$$\hat{f}(r; \rho, L, q, N) = \frac{N}{N-1} \left( \frac{1}{q} - \frac{1}{N} \right) f(r; \rho, L) \quad (4)$$

and

$$\hat{f}_0(r; L, q, N) = \frac{N}{N-1} \left( 1 - \frac{1}{q} \right) f_0(r; L). \quad (5)$$

These distributions depend weakly on the number of features  $N$ , which matters only when the features are few or in the degenerate case when they approach the number of clusters. Figures 1B and C show these distributions for two different sample sizes. When the sample size is small, the overlap between  $\hat{f}$  and  $\hat{f}_0$  is large. More samples separate the distributions and enable correct inference of the underlying clusters.

Thresholding the observed correlations to separate signal from noise trades off true and false positives. The intersection  $r_i$  between  $\hat{f}(r; \rho, L, q, N)$  and  $\hat{f}_0(r; L, q, N)$

provides a candidate optimal threshold: a lower threshold adds more outside-cluster than within-cluster correlations (more false than true positives), while a higher threshold removes more within-cluster than outside-cluster correlations (more true than false positives), as illustrated in Fig. 1B and C.

An analytical expression for  $r_i$  follows from the series expansion of Gauss' hypergeometric function:

$${}_2F_1\left(\frac{1}{2}, \frac{1}{2}, \frac{2L-1}{2}, \frac{\rho r+1}{2}\right) = 1 + \mathcal{O}\left(\frac{\rho r}{L}\right). \quad (6)$$

This series converges fast. For large sample sizes, we can use  ${}_2F_1\left(\frac{1}{2}, \frac{1}{2}, \frac{2L-1}{2}, \frac{\rho r+1}{2}\right) = 1$ . The two distributions intersect at  $r = r_i$ , where  $\hat{f}(r_i; \rho, L, q, N) = \hat{f}_0(r_i; L, q, N)$ , equivalent to

$$(1 - \frac{1}{q}) = \left( \frac{1}{q} - \frac{1}{N} \right) \frac{(1 - \rho^2)^{\frac{L-1}{2}}}{(1 - \rho r_i)^{\frac{2L-3}{2}}} \quad (7)$$

such that

$$r_i = \frac{1}{\rho} - \frac{(1 - q/N)^{\frac{2}{2L-3}} (1 - \rho^2)^{\frac{L-1}{2L-3}}}{\rho(q-1)^{\frac{2}{2L-3}}}, \quad (8)$$

the threshold with the best balance between true and false positives.

This threshold gives the probabilities for within-cluster links

$$p_{in}(\rho, L, q, N) = \int_{r_i}^1 \hat{f}(r; \rho, L) dr \quad (9)$$

and outside-cluster links

$$p_{out}(L, q, N) = \int_{r_i}^1 \hat{f}_0(r; L) dr. \quad (10)$$

The ratio  $p_{out}/p_{in}$  reveals the transition from overlapping to separated distributions. Figure 2 shows this transition

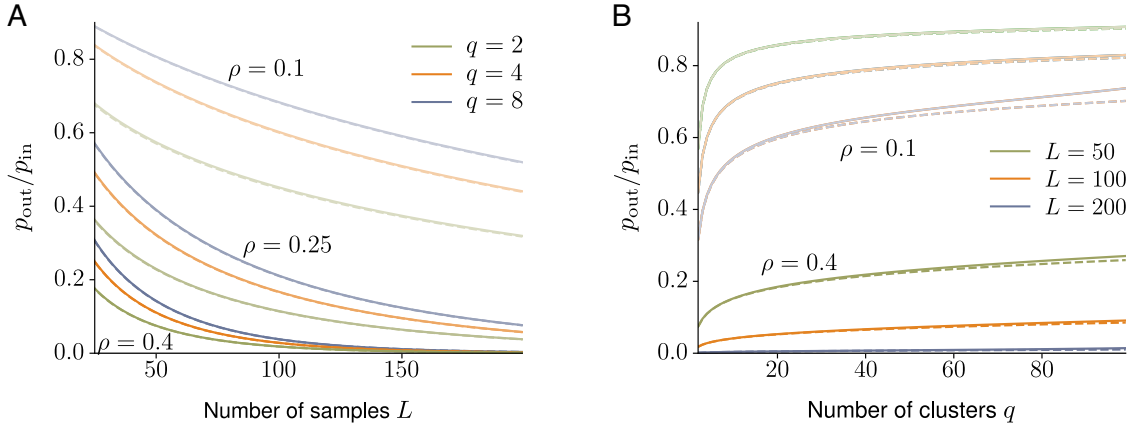


**FIG. 2. The transition to separated correlation distributions.** In A, the ratio  $p_{\text{out}}/p_{\text{in}}$  shows the non-linear transition from overlapping to separated outside- and within-cluster distributions as the number of samples  $L$  increases. More samples are required if the number of clusters  $q$  increases, particularly if the population correlation is weak. The number of nodes has a negligible effect, as shown by the barely visible dashed lines where the number of nodes is doubled. In B, splitting the network into more clusters increases  $p_{\text{out}}/p_{\text{in}}$ , making correct inference more difficult, particularly with weak correlation. The number of features matters weakly in this case, where more features actually ease inference.

as the number of samples increases (2A) and as the number of clusters increases (2B). The transition is non-linear in both samples  $L$  and clusters  $q$ . With a strong population correlation,  $p_{\text{out}}/p_{\text{in}}$  decreases sharply as samples increase, while the decrease is more gradual with a weaker population correlation. With weak population correlation, splitting the network into more clusters leads to a sharp increase in  $p_{\text{out}}/p_{\text{in}}$  with more noise (Fig. 2B), making correct inference more difficult. The number of features starts to matter in this case, with more features actually reducing the noise level somewhat. With many samples and strong correlation, the number of clusters matters less.

From a practical research perspective, if a group of features in the studied system correlates, the risk of misclassifying a link decreases non-linearly with the number of samples. This risk depends weakly on the number of observed features  $N$  and can even decrease with more features. If the system has many clusters, inference becomes more difficult compared to a system of similar size with few clusters.

### III. BAYESIAN CLUSTER-BASED REGULARIZATION

Sample size is a key limiting factor for inferring clusters in similarity data. To make better use of limited data, we capitalize on developments in network community detection methods that employ regularization with Bayesian approaches. We consider two methods for Bayesian community detection: the Regularized Map Equation [37, 38] and the Degree-Corrected Stochastic Block Model (DC-SBM) [43]. These methods incorporate prior information about network parameters and structure to obtain a posterior estimate of network communities, but use different

approaches.

The Regularized Map Equation builds on the map equation framework, which models flow on a network as a random walk [49, 51, 52], an approach that performs well in benchmark community detection [53–55]. Communities correspond to the partition that gives the shortest description of the random walker’s path, adhering to the MDL principle. The Regularized Map Equation estimates posterior transition rates of the random walker using the Dirichlet distribution as a prior distribution of the transition rates (see Materials and Methods). The Dirichlet prior prevents overfitting modular structure in sparse networks and inferring modules in random networks.

The DC-SBM uses a combinatorial approach, fitting a block model to observed network data and aims to minimize the description length of the partitioned network, also adhering to the MDL principle. Both the Regularized Map Equation and the DC-SBM give an optimal partition of the network into clusters with the corresponding description length. Neither method requires that the number of clusters be known beforehand.

For regularizing correlation networks, the MDL principle is key: as we increase regularization to get a sparser network, the principle ensures that the inferred modular structure does not result from overfitting noise. We define the description length compression  $\Delta D$  at threshold  $\tau$  as:

$$\Delta D(\tau) = \frac{D^1(\tau) - D^*(\tau)}{D^1(\tau)}, \quad (11)$$

where  $D^1(\tau)$  is the description length of an uncompressed model (with all nodes in the same cluster) and  $D^*(\tau)$  is the description length of the best partition inferred at threshold  $\tau$ . When the threshold is low, the network

is dense and has no modular structure, resulting in low compression. At high thresholds the network becomes sparser, risking overfitting of modular structure, but both methods avoid overfitting: the Regularized Map Equation through its prior on network structure (Fig. 3), and the DC-SBM through the increased information necessary to describe a more granular partition of the sparse network.

The optimal threshold  $\tau^*$  lies between the sparse and dense extremes, where the description length compression peaks and the modular signal is strongest:

$$\tau^* = \operatorname{argmax}_{\tau} \Delta D(\tau). \quad (12)$$

Figure 3A shows the compression  $\Delta D$  as a function of  $\tau$ , comparing the Regularized Map Equation, the DC-SBM and cross-validation (as described in refs. [31, 34]), averaged over 100 runs with  $L = 100$  samples, population correlation  $\rho = 0.2$ ,  $q = 4$  clusters and  $N = 256$  nodes. As expected, the compression is zero at both extremes of the threshold range. The peak compression occurs at  $\tau^* \approx 0.22$  for both the Regularized Map Equation and the DC-SBM, identifying the optimal threshold for modular structure. The standard deviation is clearly larger with cross-validation due to reduced sample size from data splitting, while the Regularized Map Equation and the DC-SBM use all available samples.

The threshold  $\tau^*$  exceeds the intersection threshold  $r_i$ , meaning that removing false positives justifies removing even more true positives. The inclusion of false positives connects nodes in different clusters, increasing the description length for both methods. When the signal of modular structure is strong, removing true positives costs little in description length. Some lost within-cluster links leave the clusters intact, showing that criticism against hard thresholding does not hold when focusing on clusters. Cross-validation uses a higher threshold because splitting the data increases noise, widening the distribution of outside-cluster correlations and requiring a higher threshold to avoid false positives.

Figure 4A-C shows the adjusted mutual information (AMI) between planted and inferred partitions as a function of the number of samples  $L$ , using the optimal threshold  $\tau^*$  for each method. Both the Regularized Map Equation and the DC-SBM recover the planted partition with fewer samples than cross-validation, illustrating the advantage of Bayesian regularization in data-scarce settings. As a reference, hierarchical clustering (details in Materials and Methods) requires more samples to reliably infer the planted structure. In the high-noise scenarios with  $q = 50$  and  $q = 100$  clusters (B and C), hierarchical clustering performs poorly since there is no clear signal of where to cut the dendrogram (see SI). Hierarchical clustering infers modular structure even when the data are pure noise, when within- and outside-cluster correlations fully overlap. The DC-SBM exhibits similar behavior, giving  $AMI > 0$  in noise-dominated settings, indicating a tendency to overfit. In contrast, the Regularized Map

Equation exhibits a clear phase transition: below a certain sample size, it detects no modular structure with zero AMI. As the signal emerges with more samples, it transitions into a detectable regime and accurately recovers the planted clusters.

The DC-SBM struggles with two challenges when working with correlational data. First, the resolution limit of the DC-SBM causes it to merge small clusters or isolated nodes into larger blocks (Fig. 4G) [56]. This underfitting leads to poor recovery particularly in the  $q = 100$  setting where modules are small. The nested version of the DC-SBM also struggles with this challenge (see SI). Second, the DC-SBM assumes link independence, leading to overfitting in networks with high clustering coefficients [44]. This problem occurs in correlation networks because they tend to close triangles [57]. In the example shown in Figure 4F, where two 50-node clusters contain many triangles, the DC-SBM overpartitions the clusters, while the Regularized Map Equation accurately recovers the planted clusters. Accounting for triangle closure in the DC-SBM does not resolve this issue (see SI), highlighting a limitation of the combinatorial method for correlation-based networks.

We conclude that the ability to correctly infer clusters from correlational data depends on the number of samples, the population correlation, the number of clusters, and, more weakly, the number of features. For certain combinations of these parameters, the distribution of outside-cluster correlations is wide and largely overlaps with the within-cluster correlation distribution, making correct inference impossible. This detectability problem relates to the detectability limit of network communities, a well-studied limit in network science [58–60]. For large and locally tree-like networks from stochastic block models, the communities become detectable when the  $p_{\text{out}}/p_{\text{in}}$  ratio drops below a threshold determined by the number of clusters and the average degree [58]. Correlation networks differ in two ways: they are not locally tree-like, and their link probabilities are not fixed but distributions that depend on the parameters  $L$ ,  $\rho$ ,  $q$  and  $N$ . Despite these differences, both detectability problems share that more clusters demand a lower  $p_{\text{out}}/p_{\text{in}}$  ratio for reliable detection.

We numerically estimate a method's detectability limit as the boundary in the  $L-\rho$  parameter space where the average AMI between the planted and inferred partitions exceeds 0.95. Figure 5 shows this limit for the evaluated methods and different numbers of clusters  $q$  in a fixed-size network ( $N=1000$ ). Hierarchical clustering performs poorly in noisy regimes and is particularly sensitive to small sample sizes. Its detectability limits diverge from  $p_{\text{out}}/p_{\text{in}}$  isolines as  $L$  decreases. The community detection methods show a similar tendency because they use higher thresholds to reduce false positives (see SI). The DC-SBM underfits small clusters by merging them and overfits large and dense clusters by splitting them. The AMI never exceeds 0.95 with  $q = 100$  clusters (Fig. 5C), and its detectability limit for  $q = 2$  clusters is pushed into

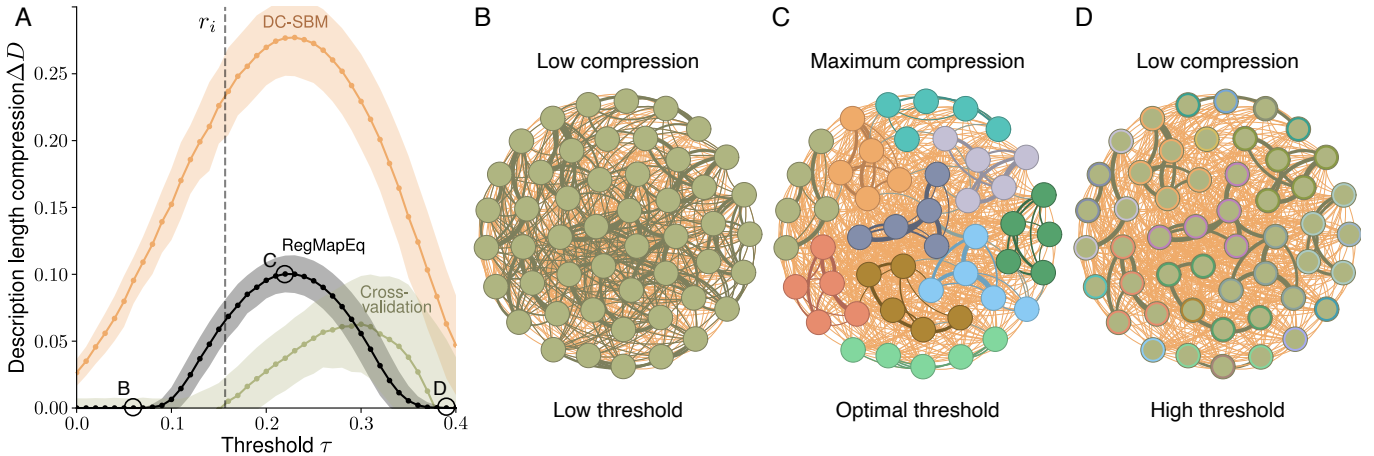


**FIG. 3. Bayesian community detection and description length compression.** In A, the description length compression peaks to the right of the intersection  $r_i$  of within- and outside-cluster correlation distributions. The compression peak lies between the dense (B) and sparse (D) networks, where the signal of modular structure is maximized (C). To avoid overfitting modular structure in sparse networks, Bayesian community detection uses a prior shown as orange, thin links in B-D. This approach regularizes correlation networks without splitting already scarce data. The node border colors in network D show the clusters without the prior.

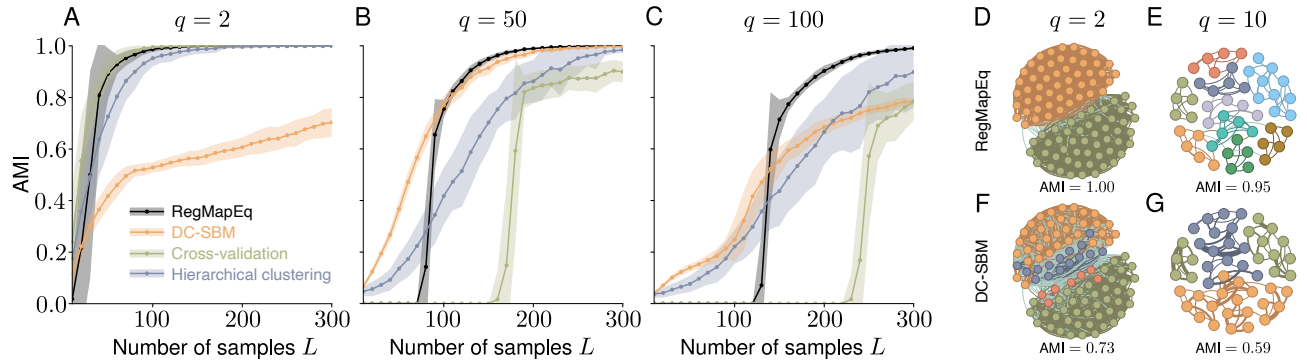


**FIG. 4. Method performance on synthetic data.** Performance measured by the adjusted mutual information (AMI) between planted and inferred partitions. For networks with  $N = 1000$  nodes, correlation strength  $\rho = 0.2$ , and  $q = 2$  clusters, the noise level is low and all methods but the DC-SBM correctly infer the planted partition using few samples (A). The DC-SBM suffers from assuming link independence while correlation networks tend to close triangles. With  $q = 50$  clusters, the Regularized Map Equation and the DC-SBM recover the planted partition with fewer samples than cross-validation and hierarchical clustering (B). With  $q = 50$  clusters, the noise level is higher, and hierarchical clustering struggles to infer the correct partition, as does the DC-SBM due to its resolution limit (C). Hierarchical clustering and the DC-SBM infer clusters ( $AMI > 0$ ) even in pure noise (B and C with few samples), making interpretation difficult. For schematic networks with  $L = 100$  samples, correlation strength  $\rho = 0.3$ , and two 50-node clusters (E, F) or ten 5-node clusters (E, G), the DC-SBM overfits the large clusters due to high clustering coefficients (F) and underfits the small clusters due to its resolution limit (G).

the low-noise region with low  $p_{out}/p_{in}$  ratio (Fig. 5A). Only in the intermediate case with  $q = 50$  clusters does it outperform cross-validation and hierarchical clustering (Fig. 5B), giving it a narrow window for application. The Regularized Map Equation's detectability limit extends into high-noise regions with relatively high  $p_{out}/p_{in}$  ratio for all tested cluster sizes (Fig. 5), recovering the planted partition even in challenging settings. Overall, the Regularized Map Equation outperforms the other methods across the tested noise levels and modular structures.

#### IV. CLUSTERS IN GENE CO-EXPRESSION DATA

With the Regularized Map Equation as the most reliable method on synthetic similarity data, we next apply it to real biological data to assess its performance in practice. We analyze transcriptomic data from the Allen Human Brain Atlas, where gene expression levels have been measured across hundreds of brain samples (details in Materials and Methods). In this more complex and noisy setting, we compare gene cluster partitions in-

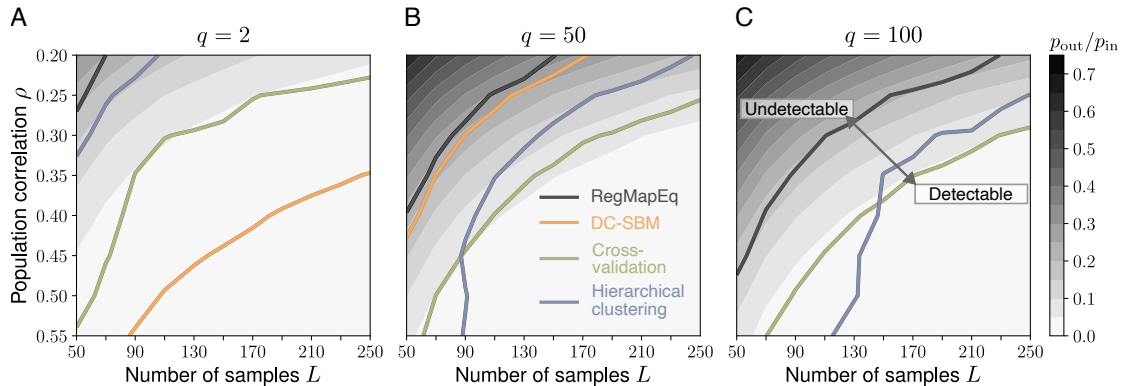


FIG. 5. **Detectability limits in the  $L - \rho$  space.** Four methods compared on network with  $N = 1000$  nodes and varying number of clusters  $q$ . Detectability defined as the line where the AMI between planted and detected partitions on average exceeds 0.95. The link ratio  $p_{\text{out}}/p_{\text{in}}$  as contour levels in the background. Cross-validation and hierarchical clustering require relatively strong signals for correct inference, and hierarchical clustering is particularly sensitive to small sample sizes. The DC-SBM works well in the intermediate case with  $q = 50$  clusters (B), where modules are neither too small nor too large and dense, but otherwise struggles with over- or underfitting. The Regularized Map Equation (RegMapEq) pushes the detectability limit furthest into the high-noise regions across all noise levels and modular structures.

ferred by the Regularized Map Equation and WGCNA, a widely used method in systems biology based on hierarchical clustering and soft thresholding [21].

WGCNA and the Regularized Map Equation produce strikingly different partitions (Fig. 6A). WGCNA assigns genes to few, relatively large clusters. In contrast, the Regularized Map Equation identifies more, smaller clusters and leaves many genes unclustered in single-gene clusters, corresponding to genes weakly correlated with others and disconnected in the underlying network. WGCNA gathers many of these weakly correlated genes in its grey cluster, which conventionally captures genes that do not co-express with others. Our analysis reveals that the other WGCNA clusters also contain many such genes, introducing noise and obscuring the inferred patterns. By using principled model selection to determine both cluster boundaries and the number of clusters, the Regularized Map Equation avoids this problem and produces coherent clusters without the noise that results from forcing all genes into multi-gene clusters.

To assess the biological relevance of the inferred clusters, we perform gene ontology (GO) enrichment analysis (see Materials and Methods). We analyze whether the enriched functions are redundant across clusters by computing the maximum Jaccard index between pairs of enriched GO term sets across all clusters for each method. WGCNA clusters exhibit substantial functional overlap across all three gene ontology categories: Biological Process (BP: 0.46), Cellular Component (CC: 0.54), and Molecular Function (MF: 0.43), indicating that many clusters share similar enriched terms, in line with the observation that they contain many uncorrelated genes. The Regularized Map Equation’s clusters are more distinct (BP: 0.10, CC: 0.13, MF: 0.05), showing clearer functional separation between clusters. The Regularized Map Equation’s clusters also show higher enrichment fac-

tors than WGCNA clusters, suggesting they more accurately capture underlying biological processes (Fig. 6B).

Finally, we examine the robustness of each method by subsampling the expression data. We reduce the number of samples available for inference and track how cluster assignments change. WGCNA shows high instability: many genes frequently change cluster when fewer samples are included (Fig. 6A). The Regularized Map Equation’s partitions are considerably more stable under the same conditions, reflected in higher AMI scores across sampling levels (Fig. 6C). These results demonstrate that the Regularized Map Equation not only identifies biologically meaningful and functionally distinct gene clusters, but also shows robustness to data sparsity. This robustness provides practical value for experimental settings where samples are often limited and expensive to collect.

## V. DISCUSSION

Standard approaches for clustering similarity data deal with noise and clustering in separate steps. This two-step approach targets clusters only in the second step, leaving clusters vulnerable to noise. When analyzing clusters is the main objective, model selection should focus directly on cluster structure. We demonstrate the advantages of this one-step approach by capitalizing on recent advances in community detection, particularly Bayesian methods that balance model complexity and fit.

We evaluated two Bayesian methods that use the Minimum Description Length principle: the Regularized Map Equation and the Degree-Corrected Stochastic Block Model. Both methods offer advantages over traditional approaches by using principled model selection that avoids inferring structure in pure noise. However, the DC-SBM assumes the observed network was

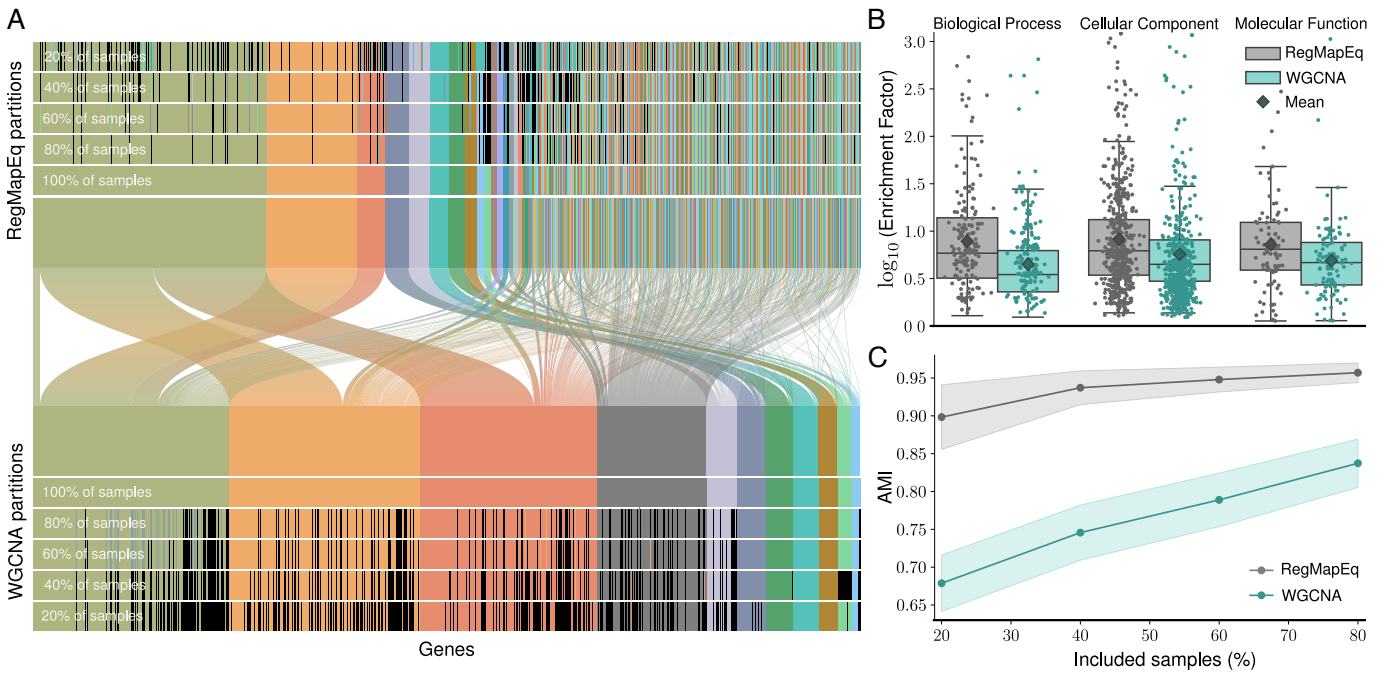


**FIG. 6. Gene clusters from gene co-expression data.** Using data from the Allen Brain Atlas, we compare gene cluster partitions inferred by WGCNA and the Regularized Map Equation. WGCNA assigns genes to large clusters (A). Its grey cluster consists entirely of uncorrelated genes as expected, but other clusters also contain many uncorrelated genes, introducing noise. In contrast, the Regularized Map Equation produces smaller, coherent clusters for correlated genes and many single-gene clusters for weakly correlated genes. The Regularized Map Equation also shows higher robustness to reduced sample sizes: fewer genes change module assignment, indicated by the black vertical lines in the subsampled partitions. Compared with WGCNA clusters, clusters identified by the Regularized Map Equation show higher enrichment factors (B), suggesting that it captures more biologically meaningful groupings. Higher AMI scores across sampling levels (C) confirm that the Regularized Map Equation requires fewer experiments to produce reliable modules.

generated by a specific model. This generative viewpoint brings assumptions not always valid for correlation data. For example, the DC-SBM assumes link independence, violated when correlation networks close triangles, leading to overfitting modular structure. In contrast, the Regularized Map Equation displays a sharp transition from non-detectable to detectable regimes as noise decreases, reliably inferring correct clusters even in significant noise from a combination of few samples, low population correlation, and a granular cluster structure.

Our application to gene co-expression data from the Allen Human Brain Atlas illustrates the practical value of this approach. The widely used WGCNA selects parameters based on scale-freeness rather than cluster structure, producing partitions with substantial functional overlap between clusters and low robustness to reduced sample sizes. In contrast, the Regularized Map Equation produces more functionally distinct and stable clusters.

Our results extend to more complex situations where clusters vary in size and correlation strength. The observed distribution of correlations becomes a superposition of all individual cluster and noise distributions. Detectability still depends on the overlap between the noise distribution and the weakest clusters. Adding clusters with stronger correlations leaves this overlap unchanged,

preserving the validity of our analysis.

Our one-step approach applies to any similarity measure without requiring access to underlying sample data. For example, the starting point can be a similarity matrix expressing species or molecular similarity. Cluster-based regularization also works in other settings, such as the graphical lasso. We have previously used cross-validation for this purpose [34], but Bayesian community detection should enable correct inference with even fewer samples and noisier data.

In summary, Bayesian community detection methods – particularly the Regularized Map Equation – offer a principled and reliable way to regularize correlation networks using a one-step approach that unites sparsification and clustering. These methods make better use of limited data and outperform standard methods, making them well suited for applications in systems biology, neuroscience, ecology, and other data-scarce domains where understanding modular organization is essential.

## VI. MATERIALS AND METHODS

### A. The Regularized Map Equation

To detect community structure in similarity data, we use the Regularized Map Equation, a Bayesian extension of the map equation framework [37, 38]. The standard map equation identifies communities by minimizing the average per-step description length of a random walker’s trajectory and works well for fully observed networks. However, incomplete link observations can bias estimates of node visit rates and transition probabilities. Since the map equation favors partitions that shorten the description of the observed walk, the absence of links can artificially reduce the description length for highly fragmented partitions, leading to the detection of small and spurious communities [37, 38]. Consequently, the description length estimated by the standard map equation cannot be interpreted as a reliable model selection criterion when networks are undersampled, unless one employs a cross-validation procedure [31].

The Regularized Map Equation mitigates this overfitting problem by interpreting the observed network as a finite sample from hidden transition probabilities that govern the random walk. In theory, repeated sampling under this model yields either binary links in an unweighted network or integer-valued link counts in a weighted multigraph. Rather than relying solely on these potentially sparse samples, the method uses a Bayesian rule to combine observed data with prior expectations specified by a Dirichlet distribution. This prior is uninformative and analytically tractable, reducing variance in estimated transition rates where observations are weak and producing a random walk process that is more robust to sampling noise [37, 38].

We construct our similarity networks from correlation values in the interval  $[0, 1]$ . Because the weighted Regularized Map Equation is formally derived for integer-valued link counts, applying it directly to correlation weights violates the underlying multinomial sampling assumption. We therefore threshold the networks and treat them as unweighted, setting links below the threshold to zero and links above the threshold to one, and apply the unweighted Regularized Map Equation. This preserves the probabilistic interpretation of the method without introducing assumptions about fractional weights. To ensure that this modeling choice has no effect on our results, we also apply the weighted Regularized Map Equation to correlation-weighted networks and find that it produces the same detected community structure.

We use the implementation provided in Infomap, which supports regularized inference with the same computational efficiency as the standard map equation [49]. For each evaluated threshold, we construct an unweighted and undirected network and set the prior connectivity parameter to its default value of  $\ln N/N$  [37].

### B. Hierarchical clustering

We perform agglomerative hierarchical clustering by using the correlation distance  $1 - r$  as distance between features. We calculate the distance  $d(u, v)$  between clusters  $u$  and  $v$  using the Farthest Point Algorithm, such that

$$d(u, v) = \max_{i,j} \text{dist}(u_i, v_j) \quad (13)$$

where  $u_i, v_j$  are features in clusters  $u, v$  respectively and  $\text{dist}(u_i, v_j)$  denotes the distance between features. At each level in the resulting tree-like structure we calculate the Within-Cluster Sum of Squares (WCSS), which measures the compactness of clusters, as

$$\text{WCSS}(q) = \sum_{i=1}^q \sum_{X_j \in C_i} \|X_j - \bar{X}_i\|^2 \quad (14)$$

where  $C_i$  denotes cluster  $i$  and  $\bar{X}_i$  is the centroid of cluster  $i$  defined as

$$\bar{X}_i = \sum_{X_j \in C_i} X_j / |C_i|. \quad (15)$$

We then obtain the WCSS values as a function of the number of clusters  $q$ , and we cut the tree at the level where the WCSS has its maximum change in slope, as illustrated in the Supporting Information.

### C. Gene co-expression data

We use normalized microarray expression data from the Allen Human Brain Atlas [61] (donor ID: 9861) and pre-process the data as described in ref. [3]. We filter genes to retain the top 10% most variable genes across brain samples, resulting in a set of 1934 genes and 946 samples for analysis. To simulate reduced experimental conditions, we construct gene expression matrices at four subsampling levels – 80%, 60%, 40% and 20% – by randomly selecting samples without replacement. At each level, we repeat the analysis across 100 independent subsamples.

We run the Regularized Map Equation as described above and in the companion notebook [62], WGCNA through the standard R package [33] with the dynamic tree cut algorithm to define modules, following ref. [3].

We assess partition robustness by comparing the full-data cluster assignments with those obtained from subsampled datasets. For each gene, we compute whether its cluster assignment under subsampling match the most similar cluster (by Jaccard index) in the full data. Those genes that match in less than 80 of the 100 subsamples are marked black to show that their cluster assignment is unstable. To quantify overall similarity between partitions, we calculate the AMI between the full and subsampled partitions.

To assess biological relevance, we perform Gene Ontology (GO) enrichment analysis using the g:Profiler software [63] through its Python package. For each method and cluster (excluding WGCNA's grey module), we compute the enrichment factor (observed / expected proportions) for significantly enriched GO terms, for all clusters with at least 10 genes.

## VII. ACKNOWLEDGMENTS

The authors thank the High Performance Computing Center North (HPC2N) at Umeå University for providing

computational resources and valuable support. We also thank M. Hawrylycz for advice on the Allen Human Brain Atlas data. MR was supported by the Swedish Research Council under grant 2023-03705.

---

[1] BS Everitt, S Landau, M Leese, D Stahl, *Cluster Analysis*. (Wiley, 2011), 5th edition.

[2] E Bullmore, O Sporns, Complex brain networks: graph theoretical analysis of structural and functional systems. *Nature Reviews Neuroscience* **10**, 186–198 (2009).

[3] MJ Hawrylycz, et al., An anatomically comprehensive atlas of the adult human brain transcriptome. *Nature* **489**, 391–399 (2012).

[4] A Barberán, ST Bates, EO Casamayor, N Fierer, Using network analysis to explore co-occurrence patterns in soil microbial communities. *The ISME Journal* **6**, 343–351 (2012).

[5] J Calatayud, M Neuman, A Rojas, A Eriksson, M Rosvall, Regularities in species' niches reveal the world's climate regions. *eLife* **10**, e58397 (2021).

[6] FT de Vries, et al., Soil bacterial networks are less stable under drought than fungal networks. *Nature Communications* **9**, 3033 (2018).

[7] MB Eisen, PT Spellman, PO Brown, D Botstein, Cluster analysis and display of genome-wide expression patterns. *Proceedings of the National Academy of Sciences* **95**, 14863–14868 (1998).

[8] YXR Wang, H Huang, Review on statistical methods for gene network reconstruction using expression data. *Journal of Theoretical Biology* **362**, 53–61 (2014).

[9] B Mishra, N Kumar, MS Mukhtar, Network biology to uncover functional and structural properties of the plant immune system. *Current Opinion in Plant Biology* **62**, 102057 (2021).

[10] MJ Wainwright, *High-dimensional statistics: A non-asymptotic viewpoint*. (Cambridge university press, 2019).

[11] PJ Huber, *Robust Statistics*. (Wiley, 1981).

[12] N Altman, M Krzywinski, Clustering. *Nature Methods* **14**, 545–546 (2017).

[13] J Žurauskienė, C Yau, pcaReduce: hierarchical clustering of single cell transcriptional profiles. *BMC bioinformatics* **17**, 140 (2016).

[14] M Allaoui, ML Kherfi, A Cheriet, "Considerably improving clustering algorithms using UMAP dimensionality reduction technique: a comparative study" in *International conference on image and signal processing*. (Springer, 2020), pp. 317–325.

[15] Y Hozumi, R Wang, C Yin, GW Wei, UMAP-assisted k-means clustering of large-scale sars-cov-2 mutation datasets. *Computers in biology and medicine* **131**, 104264 (2021).

[16] IT Jolliffe, *Principal Component Analysis*, Springer Series in Statistics. (Springer, 2002), 2nd edition.

[17] L McInnes, J Healy, N Saul, L Grossberger, UMAP: Uniform manifold approximation and projection. *Journal of Open Source Software* **3**, 861 (2018).

[18] JA Hartigan, MA Wong, Algorithm as 136: A k-means clustering algorithm. *Journal of the royal statistical society. series c (applied statistics)* **28**, 100–108 (1979).

[19] KY Yeung, WL Ruzzo, Principal component analysis for clustering gene expression data. *Bioinformatics* **17**, 763–774 (2001).

[20] X Chen, B Zhang, T Wang, A Bonni, G Zhao, Robust principal component analysis for accurate outlier sample detection in rna-seq data. *BMC bioinformatics* **21**, 269 (2020).

[21] B Zhang, S Horvath, A general framework for weighted gene co-expression network analysis. *Statistical Applications in Genetics and Molecular Biology* **4**, (2005).

[22] M van den Heuvel, C Stam, M Boersma, H Hulshoff Pol, Small-world and scale-free organization of voxel-based resting-state functional connectivity in the human brain. *NeuroImage* **43**, 528–539 (2008).

[23] C Bleker, SK Grady, MA Langston, A comparative study of gene co-expression thresholding algorithms. *Journal of Computational Biology* **31**, 539–548 (2024).

[24] O Ledoit, M Wolf, A well-conditioned estimator for large-dimensional covariance matrices. *Journal of Multivariate Analysis* **88**, 365–411 (2004).

[25] A Sboner, XJ Mu, D Greenbaum, RK Auerbach, MB Gerstein, The real cost of sequencing: higher than you think! *Genome biology* **12**, 125 (2011).

[26] P Milberg, J Bergstedt, J Fridman, G Odell, L Westerberg, Observer bias and random variation in vegetation monitoring data. *Journal of Vegetation Science* **19**, 633–644 (2008).

[27] N Masuda, ZM Boyd, D Garlaschelli, PJ Mucha, Introduction to correlation networks: Interdisciplinary approaches beyond thresholding. *Physics Reports* **1136**, 1–39 (2025).

[28] AD Perkins, MA Langston, Threshold selection in gene co-expression networks using spectral graph theory techniques. *BMC Bioinformatics* **10**, S4 (2009).

[29] M MacMahon, D Garlaschelli, Community detection for correlation matrices. *Phys. Rev. X* **5**, 021006 (2015).

[30] G Zahoránszky-Kőhalmi, CG Bologa, TI Oprea, Impact of similarity threshold on the topology of molecular similarity networks and clustering outcomes. *Journal of Chemical Informatics* **8**, 16 (2016).

[31] M Neuman, V Jonsson, J Calatayud, M Rosvall, Cross-validation of correlation networks using modular structure. *Applied Network Science* **7**, 75 (2022).

[32] JJ Jay, et al., A systematic comparison of genome-scale clustering algorithms. *BMC Bioinformatics* **13**, S7 (2012).

[33] P Langfelder, S Horvath, WGCNA: an R package for weighted correlation network analysis. *BMC Bioinformatics* **9**, 559 (2008).

[34] M Neuman, J Calatayud, V Tasselius, M Rosvall, Module-based regularization improves gaussian graphical models when observing noisy data. *Applied Network Science* **9**, 6 (2024).

[35] JG Augustson, J Minker, An analysis of some graph theoretical cluster techniques. *Journal of the Association for Computing Machinery* **17**, 571–588 (1970).

[36] M Rosvall, CT Bergstrom, Mapping change in large networks. *PLOS ONE* **5**, 1–7 (2010).

[37] J Smiljanić, D Edler, M Rosvall, Mapping flows on sparse networks with missing links. *Phys. Rev. E* **102**, 012302 (2020).

[38] J Smiljanić, C Blöcker, D Edler, M Rosvall, Mapping flows on weighted and directed networks with incomplete observations. *Journal of Complex Networks* **9**, cnab044 (2021).

[39] J Friedman, T Hastie, R Tibshirani, Sparse inverse covariance estimation with the graphical lasso. *Biostatistics* **9**, 432–441 (2008).

[40] M Yuan, Y Lin, Model selection and estimation in the Gaussian graphical model. *Biometrika* **94**, 19–35 (2007).

[41] N Meinshausen, P Bühlmann, High-dimensional graphs and variable selection with the Lasso. *The Annals of Statistics* **34**, 1436 – 1462 (2006).

[42] H Zou, T Hastie, Regularization and variable selection via the elastic net. *Journal of the Royal Statistical Society. Series B (Statistical Methodology)* **67**, 301–320 (2005).

[43] TP Peixoto, Nonparametric bayesian inference of the microcanonical stochastic block model. *Phys. Rev. E* **95**, 012317 (2017).

[44] TP Peixoto, Disentangling homophily, community structure, and triadic closure in networks. *Phys. Rev. X* **12**, 011004 (2022).

[45] J Rissanen, Modeling by shortest data description. *Automatica* **14**, 465–471 (1978).

[46] DN Reshef, et al., Detecting novel associations in large data sets. *Science* **334**, 1518–1524 (2011).

[47] N Amoroso, et al., Making sense of chemical space network shows signs of criticality. *Scientific Reports* **13**, 21335 (2023).

[48] T Leinster, CA Cobbold, Measuring diversity: the importance of species similarity. *Ecology* **93**, 477–489 (2012).

[49] J Smiljanić, et al., Community detection with the map equation and infomap: Theory and applications. arXiv [Preprint] (2024). <https://arxiv.org/abs/2311.04036>

[50] H Hotelling, New light on the correlation coefficient and its transforms. *Journal of the Royal Statistical Society. Series B (Methodological)* **15**, 193–232 (1953).

[51] M Rosvall, CT Bergstrom, Maps of random walks on complex networks reveal community structure. *Proceedings of the National Academy of Sciences* **105**, 1118–1123 (2008).

[52] D Edler, L Bohlin, M Rosvall, Mapping higher-order network flows in memory and multilayer networks with infomap. *Algorithms* **10** (2017).

[53] A Lancichinetti, S Fortunato, Community detection algorithms: A comparative analysis. *Phys. Rev. E* **80**, 056117 (2009).

[54] R Aldecoa, I Marín, Exploring the limits of community detection strategies in complex networks. *Scientific Reports* **3**, 2216 (2013).

[55] A Tandon, et al., Community detection in networks using graph embeddings. *Phys. Rev. E* **103**, 022316 (2021).

[56] TP Peixoto, Parsimonious module inference in large networks. *Phys. Rev. Lett.* **110**, 148701 (2013).

[57] E Langford, N Schwertman, M Owens, Is the Property of Being Positively Correlated Transitive? *The American Statistician* **55**, 322–325 (2001).

[58] A Decelle, F Krzakala, C Moore, L Zdeborová, Inference and phase transitions in the detection of modules in sparse networks. *Phys. Rev. Lett.* **107**, 065701 (2011).

[59] E Abbe, AS Bandeira, G Hall, Exact Recovery in the Stochastic Block Model. *IEEE Transactions on Information Theory* **62**, 471–487 (2016).

[60] S Fortunato, M Barthélémy, Resolution limit in community detection. *Proceedings of the National Academy of Sciences* **104**, 36–41 (2007).

[61] Allen Institute for Brain Science, The Allen human brain atlas (2024), <https://human.brain-map.org/static/download>, accessed 23 Aug 2024.

[62] Magnus Neuman, Model selection with the Regularized Map Equation, (2025), <https://github.com/magnusneuman/Model-selection-with-the-Regularized-Map-Equation>.

[63] U Raudvere, et al., g:Profiler: A web server for functional enrichment analysis and conversions of gene lists (2019 update). *Nucleic Acids Research* **47**, W191–W198 (2019).

## SUPPORTING INFORMATION

### Hierarchical clustering

Figure S1 shows that the cut height of a dendrogram with high noise levels (shown as few samples) cannot be determined. The normalized Within-Cluster Sum of Squares WCSS ( $WCSS(C) / \max_{C_i} WCSS(C_i)$ ) is shown as a function of the number of clusters, and we see that this curve does not have a clear elbow for high-noise data, while it has an elbow for low-noise data, and the dendrogram can then be cut at the correct number of clusters. We have used  $q = 50$  clusters,  $N = 1000$  nodes and population correlation  $\rho = 0.2$  while we have varied the number of samples

to change the noise level.

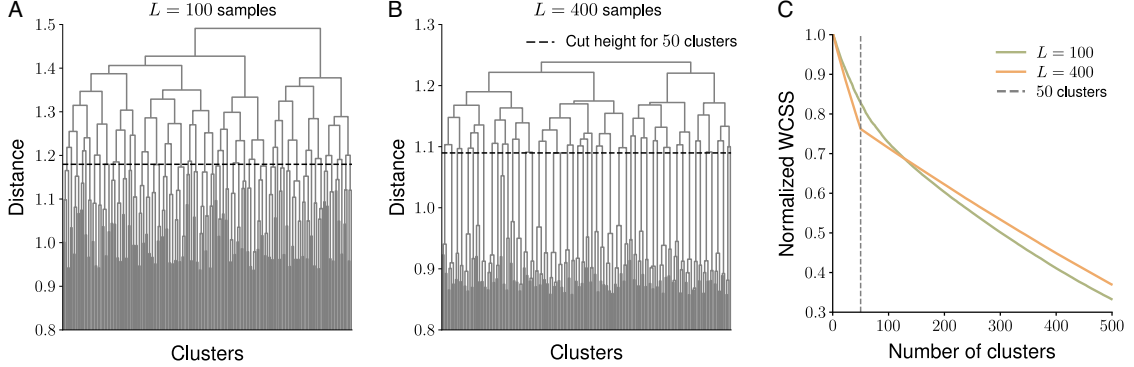


FIG. S1. The dendograms with noisy data (A,  $L = 100$  samples) and less noisy data (B,  $L = 400$  samples). With high noise the cut height of the dendrogram cannot be determined, as seen in (A) and also in (C), showing that the normalized WCSS has no clear elbow with high noise, but indeed with low noise.

### Nested DC-SBM and DC-SBM/TC

The Degree-Corrected Stochastic Block Model (DC-SBM) [S1] has a resolution limit that leads to the merging of small clusters, in this way underfitting modular structure [S2]. In Fig. S2 we show that the nested version of DC-SBM, allowing for multilevel solutions, suffers from this also.

DC-SBM has been reported to overfit modules when the network has many triangles [S3]. SBM/TC is an extension of DC-SBM to account for triangular closure [S3]. SBM/TC more accurately estimates the clustering coefficient (Fig. S3) but still fails to recover the planted clusters since we get adjusted mutual information  $AMI = 0.57$  and seven clusters for two planted 50-node clusters, which is worse than DC-SBM ( $AMI = 0.73$  and four clusters).

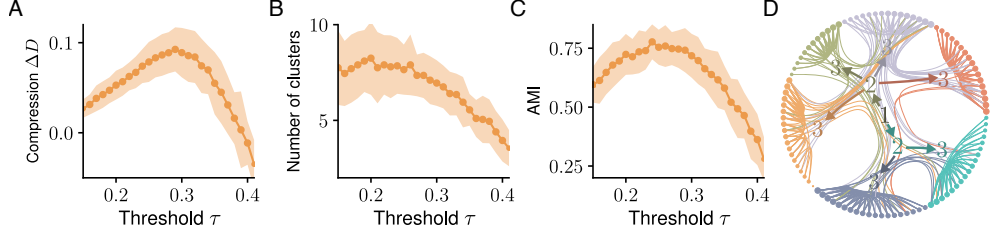


FIG. S2. Just as the 2-level DC-SBM, the nested SBM underfits modular structure in networks with small clusters, as shown here with 10 planted clusters with 10 nodes each and 50 samples of correlational data sampled from a multivariate normal distribution. The description length compression  $\Delta D$  peaks at the threshold ( $\tau = 0.29$ ) that gives the best balance between over- and underfitting modular structure to data (A). The number of clusters is less than the 10 planted clusters for all thresholds (B). The  $AMI$  between planted and inferred partitions never reaches one (C). We have compared the clusters at the bottom level in the partition tree with the planted modules. In (D) we show an instance of the partition inferred using the nested SBM together with the partition hierarchy, with the levels indicated by the numbers. We see that the nested SBM merges planted clusters into larger clusters, in line with the results obtained for the 2-level DC-SBM.

### Method thresholds are higher than $r_i$

At the intersection  $r_i$  between the within- and outside-cluster correlation distributions we have the best balance between false and true positives since increasing the threshold leads to removing more true than false positives. However, the model selection methods based on community detection that we propose converge to a higher threshold since connecting different clusters with false positives is more expensive, in terms of description length, than removing

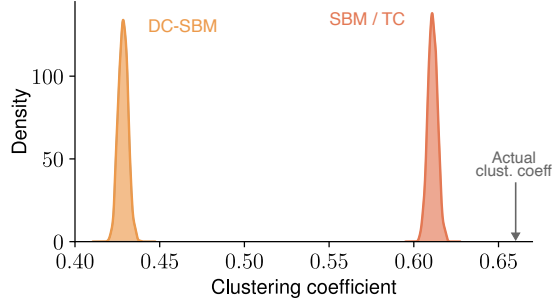


FIG. S3. The global clustering coefficient in the network with two 50-node clusters, based on  $L = 50$  samples, with the optimal threshold  $\tau^* = 0.26$  for DC-SBM, is 0.66 (arrow). The distributions of this clustering coefficient in the models inferred using DC-SBM and SBM/TC respectively do not coincide. The distribution of SBM/TC is closer to the actual value, but this is apparently not sufficient to avoid overfitting modular structure since SBM/TC infers seven clusters in our two-cluster planted network, resulting in  $AMI=0.57$ , which is worse than DC-SBM ( $AMI = 0.63$  and four clusters).

true positives, which connect nodes in already densely connected clusters. At a higher threshold  $r_i + \epsilon$  we get

$$p'_{\text{in}}(\rho, L, q, N) = \int_{r_i + \epsilon}^1 \hat{f}(r; \rho, L, q, N) dr \quad (16)$$

and

$$p'_{\text{out}}(L, q, N) = \int_{r_i + \epsilon}^1 \hat{f}_0(r; L, q, N) dr \quad (17)$$

as the probabilities for within- and outside-cluster links. Comparing the fraction  $p'_{\text{out}}/p'_{\text{in}}$  to  $p_{\text{out}}/p_{\text{in}}$ , where we use the threshold  $r_i$ , in the  $L - \rho$  space, we see that the isolines change and better resemble the detectability limits of the methods we evaluate (Fig. S4). The deviation between  $p_{\text{out}}/p_{\text{in}}$  and the methods can thus depend on the higher threshold  $r_i + \epsilon$  that we use with the methods.

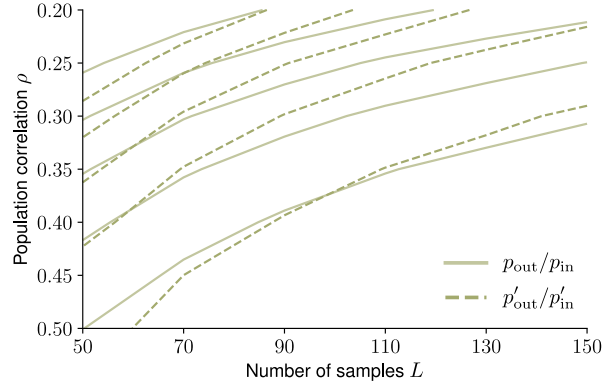


FIG. S4. The isolines of  $p'_{\text{out}}/p'_{\text{in}}$  differ from those of  $p_{\text{out}}/p_{\text{in}}$  since we use a higher threshold  $r_i + \epsilon$  when calculating  $p'_{\text{out,in}}$ . The methods we evaluate use higher thresholds and the detectability limits of the methods better resemble the isolines of  $p'_{\text{out}}/p'_{\text{in}}$  than those of  $p_{\text{out}}/p_{\text{in}}$ , so the higher threshold can explain the shape of the detectability limits in the  $L - \rho$  space. In this figure we have used  $q = 50$  clusters,  $N = 1000$  nodes and  $\epsilon = 0.05$ .

---

[S1] TP Peixoto, Nonparametric bayesian inference of the microcanonical stochastic block model. *Phys. Rev. E* **95**, 012317 (2017).  
[S2] TP Peixoto, Parsimonious module inference in large networks. *Phys. Rev. Lett.* **110**, 148701 (2013).

[S3] TP Peixoto, Disentangling homophily, community structure, and triadic closure in networks. *Phys. Rev. X* **12**, 011004 (2022).